Paper 125

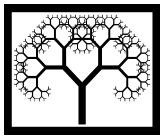

Proceedings of the Eighth International Conference on Engineering Computational Technology, B.H.V. Topping, (Editor), Civil-Comp Press, Stirlingshire, Scotland

Fast and Reduced Full-System Finite Element Solution of Line Contact Elastohydrodynamic Lubrication Problems

W. Habchi and J. Issa
Department of Industrial and Mechanical Engineering
Lebanese American University, Byblos, Lebanon

Abstract

This paper presents a reduced full-system finite element solution of elastohydrodynamic lubrication (EHL) problems. It aims to demonstrate the feasibility of this approach by applying it to the simple isothermal Newtonian line contact case. However the proposed model can be easily extended to more complex situations. This model is based on a full-system finite element resolution of the EHL equations: Reynolds, linear elasticity and load balance. A reduced model is proposed for the linear elasticity problem. For this, a novel "EHL-basis" model order reduction technique is introduced. The latter requires only a few degrees of freedom to compose the elastic deformation of the solid components. In addition, a comparison with the full model shows an order of magnitude cpu time gain with errors of the order of only 1‰ for the central and minimum lubricant film thicknesses.

Keywords: elastohydrodynamic lubrication, finite elements, model reduction, full-system approach.

1 Introduction

Lubrication has been a topic of interest for the engineering community during the last century. In particular, elastohydrodynamic lubrication (EHL) has gained much attention since its recognition as the main physical mechanism behind the successful operation of important mechanical elements such as roller bearings and transmission gears. Numerical modeling of this lubrication regime has always faced major difficulties mostly related to the high dependence of common lubricant's viscosities on pressure and the relatively large elastic deformations of the contacting elements. In fact, these contacts can be subject to very high pressures that can reach several GPa and the film thicknesses involved can go down to a few nanometers. These difficulties have lead throughout the years to the introduction of different numerical

approaches with one aim which is to have a robust and fast EHL solver that would cover a large range of operating conditions. All these approaches fall within two major categories: semi-system and full-system. In the first, the different EHL equations are solved separately and an iterative procedure is established between their respective solutions. The weak coupling in these models leads to a loss of information that is compensated by underrelaxation, leading to slow convergence rates. Many examples of such models can be found in the literature. One of the first works using this approach was that of Dowson and Higginson [1] followed by the pioneering work of Hamrock and Dowson [2]. In the Full-System approach, EHL equations are solved simultaneously, preventing any convergence degradation due to losses of information resulting from coupling. One of the first models to use such an approach is that of Rhode and Oh [3] who solved the EHL problem (in a finite element framework) as one integro-differential equation using a Newton-Raphson procedure. Later on, a similar work was provided by Houpert and Hamrock [4]. More recently, Hughes et al. [5] used the differential deflection method [6] in order to solve the EHL problem using the finite element method within a full-system framework.

Although the full-system based models mentioned above provide attractive convergence properties, these have always suffered from three major drawbacks. First, the tedious implementation of the cavitation condition because of the simultaneous solution of all pressure updates. Second, the elastic deflection calculation in these models is based on a half-space approach. Therefore, the elastic deflection at any discretization point is related to all other points of the computational domain by means of an integral calculation. This results in a full Jacobian matrix that requires an important computational overhead in order to invert it. Finally, for heavily loaded contacts, the Jacobian matrix becomes almost singular which makes the solution hard to reach. In a recent work, Habchi et al. [7], [8], [9] introduced a finite element full-system approach where the elastic deflection calculation is based on a linear elasticity model. This lead to a sparse Jacobian matrix since every discretization point belonging to a certain number of finite elements is only connected to its neighbouring points belonging to these elements. Thus the problem of the large computational overhead associated to the inversion of a full Jacobian matrix was overcome. In addition, the authors used a penalty method as proposed by Wu [10] to deal with the free boundary problem. This method is implemented in a straightforward manner, by adding an additional penalty term to the Reynolds' [11] equation. Finally, special stabilized finite element formulations were introduced for the solution of highly loaded contacts. Hence, all difficulties associated so far to the Full-System approach were overcome, allowing this model to take full advantage of its fast convergence properties. In addition, this model was shown to have the same complexity as state of the art ones, but faster convergence rates. Furthermore, the use of the finite element method which enables non-regular non-structured meshing lead to smaller size systems and hence faster solutions.

Although the model discussed above provides interesting performance properties compared to existing ones, a major improvement is possible and highly desirable to tackle computationally demanding problems (e.g. point contacts, transient EHL problems…). In fact, as stated earlier, the elastic deflection of the solid elements is

computed by means of a linear elasticity approach. The latter is applied to the entire solid domain, whereas for the EHL solution, only the surface deflection in the contact area is needed. Hence, a large number of degrees of freedom (dof) that is being computed is not useful in practice. The aim of this paper is to improve the elastic deflection calculation by reducing the size of the corresponding model. This is achieved by applying a modal-like reduction technique. For the scope of this work, which aim is to demonstrate the feasibility of such an approach, only line contacts operating under steady-state regime shall be considered. The lubricant is assumed to have a Newtonian behavior, thermal effects are neglected, and solid surfaces are taken to be smooth.

2 EHL theory and equations

Line contacts take place between two solid elements having an infinite radius of curvature in one of the principal space directions (*y*-direction). Such contacts can be reduced to an equivalent contact between a cylinder and a flat surface with the cylinder having an equivalent radius of curvature R in the *x*-direction as shown in Figure 1. The surfaces of these elements are pressed against each other by an external applied force F, they are separated by a full lubricant film and have constant unidirectional surface velocities in the *x*-direction.

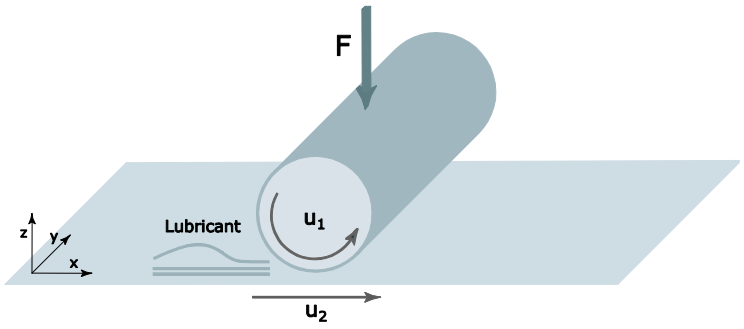

Figure 1: Geometrical description of a line contact

Three main equations define an EHL problem: the Reynolds equation which describes the pressure distribution p in the contact area, the linear elasticity equations which determine the elastic deformation of the contacting elements and the load balance equation which ensures that the correct load F is applied. All equations are written in dimensionless form using the Hertzian dry contact parameters [12] (i.e. Hertzian contact pressure p_h and Hertzian contact half-width a). The Reynolds [11] equation describing the dimensionless pressure distribution P for a steady-state line contact problem with unidirectional surface velocities u_1 and u_2 in the X-direction is given by:

$$\frac{\partial}{\partial X}\left(\varepsilon\frac{\partial P}{\partial X}\right)-\frac{\partial\left(\bar{\rho}H\right)}{\partial X}=0 \qquad (1)$$

Where: $\varepsilon = \dfrac{\bar{\rho} H^3}{\bar{\mu}\lambda}$, $\lambda = \dfrac{12 u_m \mu_R R^2}{a^3 p_h}$ and $u_m = \dfrac{u_1 + u_2}{2}$

This equation stems from the Navier-Stokes equations to which the thin film simplifying assumptions are applied. H is the film thickness. The dimensionless viscosity $\bar{\mu}$ and density $\bar{\rho}$ vary with pressure throughout the contact domain Ω_c (See Figure 2) making the problem highly nonlinear.

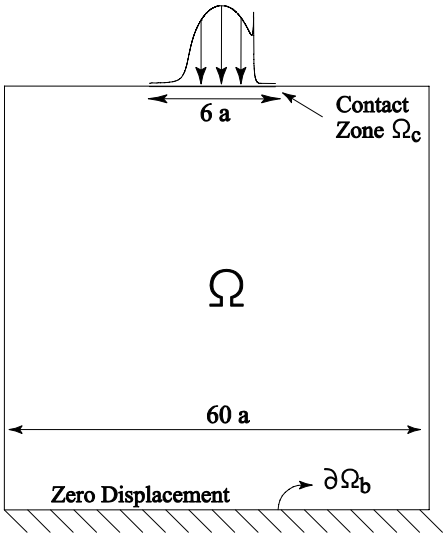

Figure 2: Computational domain of the line contact problem

The modified WLF model proposed by Yasutomi et al. [13] is used for viscosity variations with respect to pressure:

$$\mu(p) = \mu_g \times 10^{\frac{-C_1 (T_0 - T_R(p)) F(p)}{C_2 + (T_0 - T_R(p)) F(p)}} \tag{2}$$

With: $T_g(p) = T_g(0) + A_1 \ln(1 + A_2 p)$ and $F(p) = 1 - B_1 \ln(1 + B_2 p)$

Where T_0 is the ambient temperature. As for density variations with pressure, the Dowson and Higginson [14] model is used:

$$\rho(p) = \rho_R \left(1 + \frac{0.6 \times 10^{-9} p}{1 + 1.7 \times 10^{-9} p} \right) \tag{3}$$

Neglecting body loads, the linear elasticity equations consist in finding the displacement vector $U = \{u, v\}$ over the *2D* computational domain Ω such that:

$$div(\sigma) = 0 \ with \ \sigma = C \varepsilon_s(U) \tag{4}$$

Where σ is the stress tensor, ε_s the strain tensor and C the compliance matrix. Line contacts being infinitely long in the *y*-direction, a plane-strain approximation is

assumed. The computational domain Ω of the linear elasticity problem is a square which edges are large enough compared to the contact area (See Figure 2) in order to satisfy the half-space approximation and avoid any side effects. An edge length of at least 60*a* was shown to be sufficient [7]. In order to simplify the computational model, an equivalent problem is defined to replace the elastic deformation computation for both contacting bodies under the same pressure distribution. The equivalent model is defined by applying eq. (4) to a body that has the following material properties [7][8], [9]:

$$E_{eq} = \frac{E_1^2 E_2 \left(1+\upsilon_2\right)^2 + E_2^2 E_1 \left(1+\upsilon_1\right)^2}{\left[E_1\left(1+\upsilon_2\right) + E_2\left(1+\upsilon_1\right)\right]^2} \times \frac{a}{R\, p_h}$$
$$\upsilon_{eq} = \frac{E_1\upsilon_2\left(1+\upsilon_2\right) + E_2\upsilon_1\left(1+\upsilon_1\right)}{E_1\left(1+\upsilon_2\right) + E_2\left(1+\upsilon_1\right)} \tag{5}$$

The previous simplification is equivalent to considering that one of the bodies is rigid while the other accommodates the total elastic deflection of both surfaces. This avoids running a similar calculation twice (once for every solid body). The film thickness *H* contains three contributions: the rigid body separation H_0, the original undeformed geometrical shape and the elastic deflection of the solid components δ:

$$H\left(X\right) = H_0 + \frac{X^2}{2} + \delta\left(X\right) \quad with \quad \delta\left(X\right) = \left|v\left(X\right)\right| \tag{6}$$

Finally, the load balance equation is written in dimensionless form as follows:

$$\int_{\Omega_c} P\left(X\right) dX = \frac{\pi}{2} \tag{7}$$

Where $\pi/2$ corresponds to the dimensionless external load. This equation ensures that the correct external load *F* is applied. The latter is controlled by the value of the film thickness constant H_0. To complete these equations, boundary conditions must be supplied for Reynolds' and the linear elasticity equations. For Reynolds' equation, the pressure is considered to be zero at the boundaries of the contact area:

$$P = 0 \quad on \quad \partial\Omega_c \tag{8}$$

As for the complementary film rupture boundary condition, which is used to define the free exit boundary of the contact:

$$P \geq 0 \, on \; \Omega_c \; and \; P = \nabla P \cdot \vec{n}_c = 0 \quad on \, the \, cavitation \, boundary \tag{9}$$

Where $\vec{n}_c$ is the outward normal vector to the outlet boundary of the contact. Finally, the boundary conditions of the elastic problem are defined as follows:

$$\begin{cases} U = 0 & at \, the \, bottom \, boundary \, \partial\Omega_b \\ \sigma_n = \sigma \cdot \vec{n} = -P & at \, the \, contact \, area \, boundary \, \Omega_c \\ \sigma_n = 0 & elsewhere \end{cases} \tag{10}$$

3 Full and Reduced Models

The full model for line contact problems has been previously introduced in [7], [8], [9] and in this section only a brief reminder of this model shall be provided. Both the full and reduced models are based on the Full-System finite element approach introduced in [7], [8], [9]. The three EHL equations (Reynolds, elasticity and load balance) are solved simultaneously using a damped Newton procedure as described in [15]. The free boundary problem is treated by means of a penalty method as proposed by Wu [10]. The latter consists in adding a penalty term to the Reynolds equation. This term acts only in the negative pressure region and forces the negative pressures towards zero. Reynolds equation thus becomes:

$$\frac{\partial}{\partial X}\left(\varepsilon\frac{\partial P}{\partial X}\right)-\frac{\partial\left(\bar{\rho}H\right)}{\partial X}-\xi\cdot P^{-}=0 \tag{11}$$

Where ξ is an arbitrary large positive number and $P^{-}=\min\left(P,0\right)$ corresponds to the negative part of the pressure distribution. In addition, for heavily loaded contacts, the stabilized Galerkin least squares (GLS) finite element formulation introduced in [9] is used. The need for a stabilized formulation stems from the fact that Reynolds equation can be written as a convection-diffusion-reaction equation by splitting the first order term in two [9]. And for heavy loads, this equation becomes convection-dominated which necessitates the use of special stabilized formulations to avoid the spurious behavior obtained using a standard Galerkin formulation.

3.1 Full Model

In the full model, the linear elasticity equations (4) are applied to the entire solid geometrical domain Ω, whereas Reynolds' equation is applied only to the one-dimensional contact area Ω_c. On the other hand, the load balance equation is an ordinary integral equation that is added directly to the system of equations formed by the Reynolds and linear elasticity equations, along with the introduction of an additional unknown H_0. The weak form finite element formulation of the obtained system of equations reads:

$$\begin{aligned}&Find\left(U,P,H_0\right)\in S_U\times S_P\times\mathbb{R}\ such\,that\ \forall\left(W_U,W_P,W_{H_0}\right)\in S_U\times S_P\times\mathbb{R}:\\&\begin{cases}\int_{\Omega}-C\epsilon_s\left(U\right)\cdot\epsilon_s\left(W_U\right)d\Omega+\int_{\Omega_c}-P\cdot\vec{n}\,W_U d\Omega=0\\\int_{\Omega_c}-\epsilon\frac{\partial P}{\partial X}\frac{\partial W_P}{\partial X}d\Omega+\int_{\Omega_c}\bar{\rho}H\frac{\partial W_P}{\partial X}d\Omega-\int_{\Omega_c}\xi\cdot P^{-}W_P\,d\Omega=0\\\int_{\Omega_c}PW_{H_0}d\Omega-\frac{\pi}{2}W_{H_0}=0\end{cases}\end{aligned} \tag{12}$$

Where: $S_U = \left\{ U \in H^1(\Omega) / U = 0 \text{ on } \partial\Omega_b \right\}$ and $S_P = \left\{ P \in H^1(\Omega_c) / P = 0 \text{ on } \partial\Omega_c \right\}$

Let us now write the discrete form of the previous system of equations. Consider $\Omega^h = \left\{ \Omega_1, \ldots, \Omega_{n_e} \right\}$ a finite element partition of Ω such that: $\bar{\Omega} = \cup_{e=1}^{n_e} \bar{\Omega}_e$, $\bar{\Omega} = \Omega \cup \partial\Omega$, $\bar{\Omega}_e = \Omega_e \cup \partial\Omega_e$ and $\Omega_e \cap \Omega_{e'} = \phi$ if $e \neq e'$. n_e denotes the total number of elements in the partition while $\partial\Omega$ and $\partial\Omega_e$ denote respectively the boundaries of the domain Ω and the element Ω_e. Let Ω_{ce} be the set of elements representing the *1D* contact domain Ω_c and defined by $\Omega_{ce} = \left\{ \Omega_e \cap \Omega_c / \Omega_{ce} \neq \varnothing \right\}$ and let n_{ce} be the total number of elements belonging to Ω_{ce}. Let $S_U^h \subset S_U$ and $S_P^h \subset S_P$. The discrete functions U^h and P^h defining these spaces have the same characteristics as their analytical equivalents U and P with the only difference that $U^h \in L^l$ and $P^h \in L^l$ where L^l is the set of interpolation polynomials of degree l defined within each element Ω_e. The discrete form of the previous system of equations is obtained by replacing the field variables U and P by their discrete equivalents $U^{h^{(e)}}$ and $P^{h^{(e)}}$ within every element *e*:

$$U^{h^{(e)}} = \sum_{i=1}^{n_U} U_i^{(e)} N_{U_i} \quad and \quad P^{h^{(e)}} = \sum_{i=1}^{n_p} P_i^{(e)} N_{P_i} \tag{13}$$

Where $U_i^{(e)}$ and $P_i^{(e)}$ are the nodal values of U and P respectively, associated to the interpolation functions N_{Ui} and N_{Pi} within the element *e* (n_U and n_P being their respective numbers). Similarly, the weighting functions W_U and W_P are approximated by $W_U^{h^{(e)}}$ and $W_P^{h^{(e)}}$ respectively:

$$W_U^{h^{(e)}} = \sum_{i=1}^{n_U} W_{U_i}^{(e)} N_{U_i} \quad and \quad W_P^{h^{(e)}} = \sum_{i=1}^{n_p} W_{P_i}^{(e)} N_{P_i} \tag{14}$$

Where $\mathrm{W}_{U,i}^{(e)}$ and $W_{P,i}^{(e)}$ are the nodal values of the weight functions W_U and W_P within the element *e* respectively. Finally, by adding the stabilizing GLS term to Reynolds equation, the discrete form of the system of equations (12) becomes:

$$\begin{aligned} &Find \left(U^h, P^h, H_0 \right) \in S_U^h \times S_P^h \times \mathbb{R} \; such that \\ &\forall \left(W_U^h, W_P^h, W_{H_0} \right) \in S_U^h \times S_P^h \times \mathbb{R} : \end{aligned} \tag{15}$$

$$
\begin{cases}
\int\limits_{\Omega^h} -C\epsilon_s\left(U^h\right)\cdot\epsilon_s\left(W_U^h\right)d\Omega + \int\limits_{\Omega_c^h} -P^h\cdot\vec{n}\,W_U^h d\Omega = 0 \\
\int\limits_{\Omega_c^h} -\epsilon\frac{\partial P^h}{\partial X}\frac{\partial W_P^h}{\partial X}d\Omega + \int\limits_{\Omega_c^h}\bar{\rho}H\frac{\partial W_P^h}{\partial X}d\Omega \overbrace{- \int\limits_{\Omega_c^h}\xi\cdot P^{h-}W_P^h\,d\Omega}^{Penalty\ term} \\
\qquad \underbrace{-\sum_{e=1}^{n_{ce}}\int\limits_{\Omega_{ce}} R_h\left(P^h\right)\tau\left(H\frac{\partial\bar{\rho}}{\partial P}\frac{\partial W_P^h}{\partial X} - \frac{\partial}{\partial X}\left(\epsilon\frac{\partial W_P^h}{\partial X}\right)\right)d\Omega}_{GLS\ term} = 0 \\
\int\limits_{\Omega_c^h} P^h W_{H_0}\,d\Omega - \frac{\pi}{2}W_{H_0} = 0
\end{cases}
$$

Where R_h is the residual of the hydrodynamic problem (Reynolds equation). The tuning parameter τ is defined as:

$$
\begin{gathered}
\tau = \frac{h_e}{2|\beta|l}\xi\left(Pe\right) \\
with:\ \beta = H\frac{\partial\bar{\rho}}{\partial P},\ Pe = \frac{|\beta|h_e}{2\epsilon l}\ \ and\ \ \xi\left(Pe\right) = \coth\left(Pe\right) - \frac{1}{Pe}
\end{gathered}
\tag{16}
$$

Where h_e and Pe are respectively the characteristic length and the local Peclet number of the element *e*. *l* is the polynomial order of the hydrodynamic problem's Lagrange shape functions N_P. In the current work, second order Lagrange elements (l = 2) are employed for both the elastic and hydrodynamic problems (N_U and N_P). The system of equations (15) is nonlinear and a damped-Newton [15] procedure is employed in order to solve it. The latter gives rise to a linearized system of equations (as a function of the increments δU, δP and δH_0) to solve at every Newton iteration *i*:

$$
\begin{array}{c}
\qquad\qquad 2\times N_{2D} \qquad\quad N_{1D} \qquad\quad 1 \\
\begin{matrix} 2\times N_{2D} \\ N_{1D} \\ 1 \end{matrix}
\overset{i-1}{\left[\begin{array}{c|c|c}
K_{ee} & K_{eh} & \varnothing \\ \hline
K_{he} & K_{hh} & K_{hl} \\ \hline
\varnothing & K_{lh} & \varnothing
\end{array}\right]}
\overset{i}{\left\{\begin{array}{c} \delta U \\ \hline \delta P \\ \hline \delta H_0 \end{array}\right\}}
= \overset{i-1}{\left\{\begin{array}{c} R_e \\ \hline R_h \\ \hline R_l \end{array}\right\}}
\end{array}
\tag{17}
$$

The subscripts *e*, *h* and *l* stand for "elastic", "hydrodynamic" and "load balance" respectively. N_{2D} is the number of nodes in the *2D* mesh associated to the elastic problem whereas N_{1D} is the number of nodes in the *1D* mesh associated to the hydrodynamic problem. The total number of unknowns or dof of the elastic problem

is $2\times N_{2D}$ since 2 dof are associated to each node. These are δu and δv, the increments of the elastic deflections in the *x* and *z* directions respectively. On the other hand, the total number of unknowns of the hydrodynamic problem is N_{1D} since 1 dof (δP) is associated to each node. The total number of unknowns is then defined as:

$$N_{dof} = 2\times N_{2D} + N_{1D} + 1 \tag{18}$$

The matrix on the left-hand-side is the Jacobian matrix whereas the right-hand-side vector is formed by the residual vectors of the elastic, hydrodynamic and load balance equations (R_e, R_h and R_l respectively). Starting with an initial guess of the solution (Hertzian pressure distribution and its corresponding elastic deflection), the system of equations (17) is solved at every Newton iteration *i* using a direct linear system solver (UMFPACK [16]). The result is added to the solution obtained at the previous iteration according to:

$$\begin{Bmatrix} U \\ P \\ H_0 \end{Bmatrix}^i = \begin{Bmatrix} U \\ P \\ H_0 \end{Bmatrix}^{i-1} + \lambda_i \begin{Bmatrix} \delta U \\ \delta P \\ \delta H_0 \end{Bmatrix}^i \tag{19}$$

Where $\lambda_i \in [0,1]$ is a "damping factor" computed according to [15]. This operation is repeated until convergence of the solution is obtained. The convergence criteria are also provided in [15].

Remark: Note that the elastic problem and the load balance equation are linear. Hence, their corresponding contributions to the Jacobian matrix K_{ee}, K_{eh} and K_{lh} remain unchanged throughout the nonlinear resolution procedure. These matrices are only assembled once (at the 1st iteration), and the result is used throughout the iterative procedure.

3.2 Reduced Model

Although the model described above has been shown to have the same complexity as state of the art EHL solvers with faster convergence rates and smaller size systems, leading to smaller cpu times (the interested reader is referred to [7], [8], [9]), a major improvement is yet to be achieved. In fact, the elastic problem is solved over the sufficiently large two-dimensional geometrical domain associated to the solid elements. However, in practice, only the elastic deflection in the one-dimensional contact area Ω_c is needed for the EHL solution. Hence, a large number of dof is being computed in vain. The idea here is to make the elastic calculation more efficient by reducing the size of its corresponding model.

The reduced model is obtained by a simple change of solution space. In fact, the finite element formulation (15) remains the same with the only difference that the solution space S_U for the elastic problem is now replaced by a reduced "richer" one $\tilde{S}_U$. The latter has the same properties as S_U, but is formed by a smaller set of

functions. However, these functions are now defined over the entire two-dimensional geometrical domain Ω, contrarily to those forming S_U which, for a given element Ω_e, are only defined inside the element and take a value of zero elsewhere. This property is the main reason behind the richness of $\tilde{S}_U$ compared to S_U. Let N_m be the total number of functions φ^i (i=1, 2, … , N_m) forming $\tilde{S}_U$. From this point on, these functions are referred to as "basis functions" and the vectors describing their discrete form over the two-dimensional mesh of the elastic problem are referred to as "basis vectors". Now, the elastic deflection U can be formed as a linear combination of the basis functions:

$$U = \sum_{i=1}^{N_m} \alpha_i \varphi^i \tag{20}$$

Where the parameters α_i are known as "generalized coordinates". Equation (20) can be written in discrete form (within an element e) as:

$$U^{h^{(e)}} = \sum_{i=1}^{N_m} \alpha_i \varphi^{i,h^{(e)}} \tag{21}$$

Where $\varphi^{i,h^{(e)}}$ is the discrete equivalent of φ^i defined over the element e as:

$$\varphi^{i,h^{(e)}} = \sum_{j=1}^{n_U} \varphi_j^{i^{(e)}} N_{Uj} \tag{22}$$

Where $\varphi_j^{i^{(e)}}$ (j = 1…n_U) are the nodal values of φ^i within element e. Hence, the reduced discrete system of equations is now obtained by replacing U, P, W_U and W_P by their discrete equivalents $U^{h^{(e)}}$ (given by eq.(21)), $P^{h^{(e)}}$, $W_U^{h^{(e)}}$ and $W_P^{h^{(e)}}$. The unknowns of the elastic problem are now the generalized coordinates α_i. Their number is N_m compared to $2 \times N_{2D}$ in the full model case. And the matrix form of the linearized system of equations to solve at every Newton iteration i now becomes:

$$\begin{array}{c} \\ N_m \\ N_{1D} \\ 1 \end{array} \begin{array}{c} \begin{array}{ccc} \overleftarrow{N_m} & \overleftarrow{N_{1D}} & \overleftarrow{1} \end{array} \\ \left[\begin{array}{c|c|c} \tilde{K}_{ee} & \tilde{K}_{eh} & \varnothing \\ \hline \tilde{K}_{he} & K_{hh} & K_{hl} \\ \hline \varnothing & K_{lh} & \varnothing \end{array}\right]^{i-1} \end{array} \left\{\begin{array}{c} \delta\alpha \\ \hline \delta P \\ \hline \delta H_0 \end{array}\right\}^{i} = \left\{\begin{array}{c} \tilde{R}_e \\ \hline R_h \\ \hline R_l \end{array}\right\}^{i-1} \tag{23}$$

With: $\tilde{K}_{ee} = \Phi^T K_{ee} \Phi$, $\tilde{K}_{eh} = \Phi^T K_{eh}$ and $\tilde{K}_{he} = K_{he} \Phi$

$\tilde{R}_e$ is the residual of the reduced elastic problem whereas Φ is the $2N_{2D} \times N_m$ transformation matrix which columns correspond to the basis vectors.

Remark: Note that the reduced elastic problem remains linear, and therefore its corresponding contributions to the Jacobian matrix $\tilde{K}_{ee}$ and $\tilde{K}_{eh}$ are also assembled only at the 1st iteration of the nonlinear resolution procedure.

It is clear that the total number of dof of the reduced model is:

$$\tilde{N}_{dof} = N_m + N_{1D} + 1 \tag{24}$$

Hence, if one can define a sufficiently rich solution space $\tilde{S}_U$ such that the total number of basis functions required to reconstitute any EHL elastic deformation (within a wide range of operating conditions) $N_m \ll 2 \times N_{2D}$, then the size of the reduced model $\tilde{N}_{dof} \ll N_{dof}$. As a consequence, cpu times are expected to be reduced.

Now that the basic principles behind the reduced model employed in this work have been introduced, the whole problem boils down to choosing an appropriate reduced solution space $\tilde{S}_U$. Model reduction of linear elasticity problems in itself is not a novel topic. In fact, numerous techniques can be found in the literature for the selection of the reduced solution space. The interested reader is referred to [17] and references therein for an exhaustive review of these techniques. In this work, three model reduction techniques have been inspected. The first two are more or less classical: a "modal coordinate reduction" technique also known as "modal reduction" [18], which uses the mode shapes of a structure in order to form its reduced solution space and a "Ritz-vector-like" [19] method which uses some load dependent deflections as basis vectors. Finally, the third method is a novel EHL-oriented one, which uses EHL deflections as basis vectors. The classical approaches turned out to be inefficient since they require an extremely large number of basis functions N_m to attain an acceptable solution. In fact, the function decomposition technique suggested in eq. (20) is known to generate micro-oscillations in the desired solution when a large number of basis functions is employed. In most applications this can be tolerated. However, for the EHL problem, the elastic deformations of the solid components are often several orders of magnitude larger than the lubricant film thickness. Hence, the slightest error in the elastic deflection has an important effect on the film thickness. In addition, since the latter appears to the cubic power in the second order term of Reynolds equation, this effect is even more amplified on pressure. The test results for the modal reduction and Ritz-vector-like methods will not be shown in this paper. The interested reader is referred to [20] for further details.

Based on the unsatisfactory results obtained by the classical modal reduction and Ritz-vector like methods, it is unavoidable to adopt a more "EHL-oriented" strategy in the choice of basis functions for the reduced model. In this section, a novel

method is proposed, where the basis functions are nothing else but EHL elastic deflections computed using the full model presented earlier. From this point on, the resulting basis is referred to as "EHL-basis". The corresponding functions are selected in such a way to cover a large range of operating conditions. The Moes [21] dimensionless load and material properties parameters, M and L respectively, are used to define this range. In fact, the EHL-basis functions are selected within a range of values $0 < M \leq 1000$ and $0 < L \leq 20$. Their selection is based on numerical experimentation and visualization of the corresponding deflections, mostly their deviation with respect to the Hertzian elastic deflection within the contact area Ω_c. The following observations were established:

1- It is important to distinguish three separate domains of operating conditions based on their values of M. These are $M \in]0,20]$, $]20,50]$ and $]50,1000]$ corresponding to Low, Medium and High values of M respectively.

2- In the High M regime, often associated to high loads, the EHL solution is very sensitive to any micro-oscillations in the elastic deflection resulting from the superposition of a large number N_m of basis functions. This is because the elastic deflection in this regime is often several orders of magnitude larger than the film thickness. As a consequence, a smaller and more scattered number of basis functions is to be employed under these conditions.

Based on the previous observations, three separate sets of basis functions were derived. These are shown in Figure 3 for the Low, Medium and High M regimes. For all three cases, the Hertzian elastic deflection is used as the first basis function. The remaining functions are marked by an x-tick in their corresponding grid showing their M and L values. The total number of basis functions N_m does not exceed 30 in all cases (N_m =29 for Low and Medium M whereas N_m =22 for high M). Finally, it is important to note that the choice of EHL-basis is not unique, however the one suggested in this work was found to provide stable solutions over the corresponding range of M and L.

	Low M			
L \ M	5	10	15	20
1	x	x	x	x
3	x	x	x	x
7	x	x	x	x
10	x	x	x	x
13	x	x	x	x
17	x	x	x	x
20	x	x	x	x

	Medium M			
L \ M	20	25	35	50
1	x	x	x	x
3	x	x	x	x
7	x	x	x	x
10	x	x	x	x
13	x	x	x	x
17	x	x	x	x
20	x	x	x	x

	High M								
L \ M	50	65	95	140	200	350	550	800	1000
1	x				x				x
2		x				x			
4			x				x		
7				x				x	
10	x				x				x
12		x				x			
14			x				x		
17				x				x	
20	x				x				x

*Hertzian elastic deflection is the first basis function in all three cases (Low, Medium and High M)

Figure 3: Composition of the EHL-basis for the Low (left), Medium (centre) and High M (right) regimes

Remark: Note that the EHL-basis functions are not orthogonal with respect to the linear elasticity stiffness matrix K_{ee}, leading to a full reduced stiffness matrix $\tilde{K}_{ee}$. However, considering their very small number (N_m<30), the total number of nonzero terms in $\tilde{K}_{ee}$ is negligible compared to K_{ee}.

In order to test this EHL-oriented method, three test cases are considered (one for each M regime). The first corresponds to M=17, L=15, p_h=1.05GPa (Low M), the second M=30, L=5, p_h=0.46GPa (Medium M) and finally M=375, L=15, p_h=4.91GPa (High M).

Figure 4 shows the dimensionless pressure and film thickness distributions obtained by both the full and reduced models for the three test cases considered. It is clear that the solutions obtained by the reduced model perfectly match those obtained by the full one and no oscillations are observed. Hence, despite the relatively small number of basis functions employed in the EHL-Basis, the latter is rich enough to allow a robust and satisfactory solution of the problem.

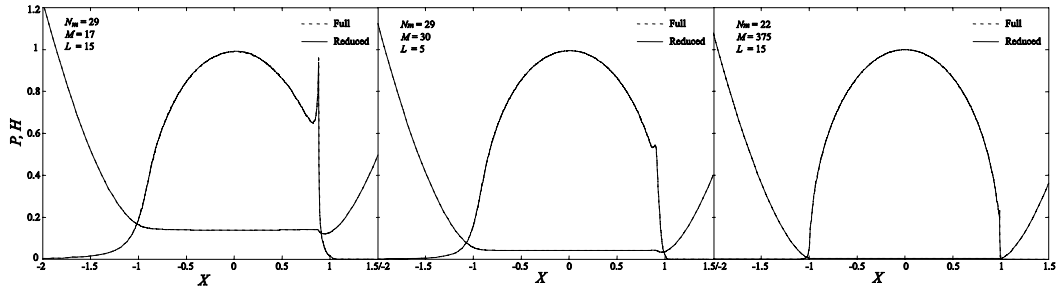

Figure 4: Dimensionless pressure and film thickness profiles obtained using the EHL-Basis method for 3 different test cases. Left: M=17, L=15, ph=1.05GPa (Low M), Centre: M=30, L=5, ph=0.46GPa (Medium M), Right: M=375, L=15, ph=4.91GPa (High M)

From this point on, only the EHL-Basis method is adopted and a thorough investigation of its numerical properties is realized.

4 Results

In the following, motivated by the promising results obtained using the EHL-Basis technique, a thorough investigation of the numerical performance of this method is presented. Five different mesh cases are considered in this section: "*Extra Coarse*", "*Coarse*", "*Normal*", "*Fine*" and "*Extra Fine*". Their respective properties are listed in Table 1 for both the full and reduced models.

Mesh Case	N_{2D}	N_{1D}	N_{dof}	$\tilde{N}_{dof}$	
				Low / Medium M	High M
Extra Coarse	741	105	1588	135	128
Coarse	1816	203	3836	233	226
Normal	5419	499	11338	529	522
Fine	10773	909	22456	939	932
Extra Fine	63927	4229	132084	4259	4252

Table 1: Properties of the different mesh cases considered

All mesh cases are developed such that the mesh size be fine in the Hertzian contact area, coarser in the inlet and outlet regions of the contact and even coarser and coarser with increasing distance from the *1D* contact area. This guarantees a custom-tailored "EHL-optimized" dof repartition over the *2D* computational domain Ω. Figure 5 shows the "*Extra Coarse"* (left), *"Normal"* (centre) and *"Extra Fine"* (right) mesh cases.

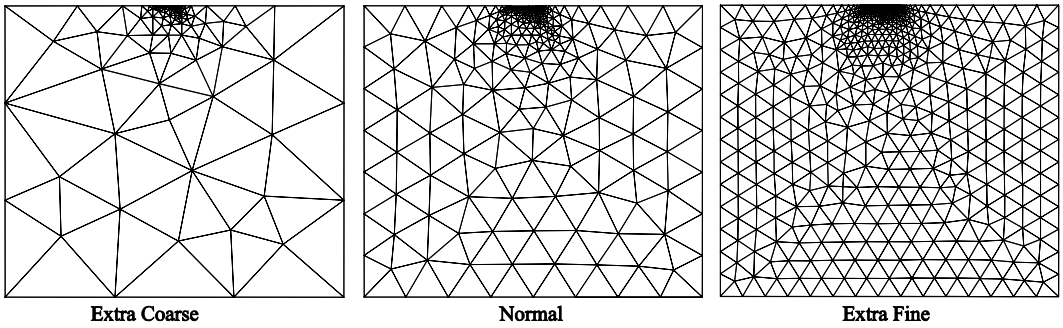

Figure 5: "Extra Coarse" (left), "Normal" (centre) and "Extra Fine" (right) mesh cases

In the following numerical tests three different lubricants are considered: a standard paraffinic mineral base oil (CPRI), a low viscosity mineral base oil (CPRP) and a synthetic hydrocarbon base lubricant of higher viscosity (PENNZ). Their modified WLF constant parameters are listed in Table 2 along with their ambient pressure viscosity μ_R and equivalent pressure-viscosity coefficient α^*. The ambient temperature is considered to be T_0=25°C.

	WLF constant parameters								μ_R	α^*
	A_1(°C)	A_2(MPa^{-1})	B_1	B_2(MPa^{-1})	C_1	C_2(°C)	$T_g(0)$ (°C)	μ_g (Pa.s)	(Pa.s)	(GPa^{-1})
CPRI	19.17	4.07x10^{-3}	0.230	0.0249	16.04	18.18	-73.86	10^{12}	0.0283	23.6
CPRP	22.47	4.22x10^{-3}	0.222	0.0349	15.87	10.22	-113.79	10^{12}	0.0016	12.5
PENNZ	69.81	1.68x10^{-3}	0.213	0.0118	11.84	60.59	-87.46	10^{7}	0.2021	18.05

Table 2: Viscosity data for CPRI, CPRP and PENNZ lubricants

Finally, all numerical tests are carried out for Steel-Steel contacts. The employed Steel has a Poisson's coefficient υ=0.3 and a Young's Modulus E=210GPa.

4.1 Convergence and complexity

In this section, the convergence properties of the proposed model with respect to the mesh size are studied along with the complexity of both the full and reduced models. In order to study the convergence of the EHL solution with respect to the mesh size, two typical EHL cases are considered M=30, L=5 (p_h=0.46GPa) and M=500, L=10 (p_h=3.78GPa). The values of the dimensionless central film thickness H_c and minimum film thickness H_{min} (obtained by the full model) are reported in Figure 6 for the five different mesh cases considered. Figure 6 (left) clearly shows that for the lightly loaded case (M=30, L=5) convergence of the central and minimum dimensionless film thicknesses is reached for the "*Normal"* mesh case. However, for the highly loaded case (M=500, L=10), convergence is reached for the *"Fine"* mesh case. This feature is common to all EHL models, since highly loaded contacts are known to be more numerically sensitive to mesh size variations. Based on these results, from this point on, unless stated otherwise, the *"Fine"* mesh case is adopted for numerical tests.

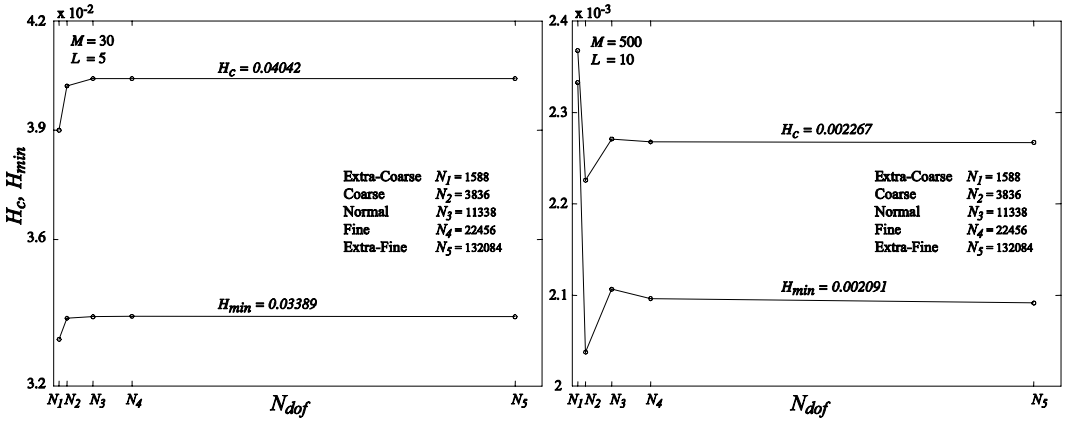

Figure 6: Solution convergence of the proposed model with respect to the mesh size

Finally, the complexity of both the full and reduced models is studied. Table 3 lists the cpu time required for one Newton iteration by both models (using a 2.4GHz processor) for a typical line contact case (M=30, L=5) as a function of the total number of dof. These results are used to plot the overall global complexity of the full and reduced model algorithms as shown in Figure 7.

Full Model		Reduced Model	
N_{dof}	t_{cpu} / Newt. Iter. (s)	$\tilde{N}_{dof}$	t_{cpu} / Newt. Iter. (s)
1588 (= n_{ref})	0.015(= t_{ref})	135 (= n_{ref})	0.004(= t_{ref})
3836	0.043	233	0.006
11338	0.135	529	0.015
22456	0.284	939	0.029
132284	2.017	4259	0.182

Table 3: cpu time for one Newton iteration as a function of the total number of dof for a typical line contact (M=30, L=5) for both the full and reduced models

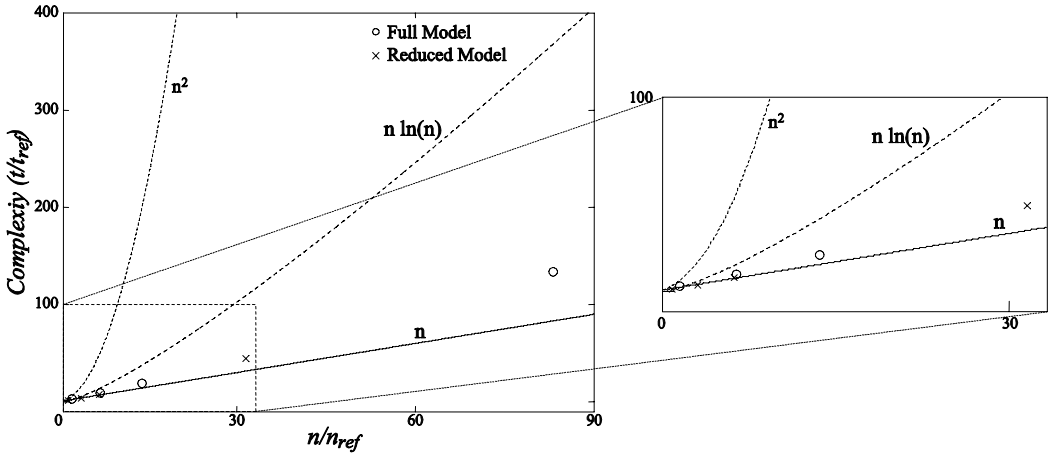

Figure 7: Complexity of the proposed full and reduced models

It is clear that both models have a complexity close to *O(n)* over a wide range of the total number of dof ($n/n_{ref} < 30$). However, as the total number of dof is further increased the complexity becomes slightly higher than *O(n)* but remains below *O(n.ln(n))* or even more $O(n^2)$ over the considered range of n/n_{ref}.

4.2 Reduced vs. full model

In this section, a series of numerical tests is realized in order to compare the precision and performance of the reduced model to that of the full one. The corresponding results are listed in Tables 4 and 5. All results discussed here are obtained using the "*Fine*" mesh case. Table 4 provides the dimensionless central film thickness H_c and minimum film thickness H_{min} obtained by both the full and reduced models for several test cases using the 3 different lubricants mentioned previously. It is clear that the relative error in H_c and H_{min} for the reduced model with respect to the full one is negligible. Despite the small number of basis functions employed, for most cases, the relative error is less than 1‰. Also note, that for lubricant CPRI, the deviations in film thickness between the reduced and full models is relatively lower than for the remaining lubricants considered here. This is probably due to the fact that CPRI lubricant was used in generating the basis functions of the reduced model.

Finally, Table 5 compares the performance of the reduced model to that of the full one in terms of convergence rates (N° of iterations required for convergence) and cpu times for the test cases considered in Table 4. The results suggest that the convergence rates of both models are virtually identical. However, although the number of iterations is practically the same, in most cases the reduced model shows an order of magnitude cpu time gain with respect to the full model. This is because of the smaller size systems obtained with the former.

	M	L	p_h	H_c			H_{min}		
			(GPA)	Full	Red.	Err.(‰)	Full	Red.	Err.(‰)
	12	12	0.70	0.18052049	0.18052302	0.014	0.15514818	0.15514674	0.009
	17	15	1.04	0.13772694	0.13771578	0.081	0.12093119	0.12083193	0.821
CPRI	45	5	0.57	0.02515687	0.02515679	0.003	0.02128733	0.02136252	3.532
	100	10	1.69	0.01438153	0.01438083	0.049	0.01290887	0.01291139	0.195
	600	8	3.31	0.00159831	0.00159830	0.006	0.00147220	0.00147069	1.026
	13	8	0.92	0.13077684	0.13074332	0.256	0.11272771	0.11259963	1.136
	40	9	1.82	0.03846414	0.03847607	0.310	0.03416566	0.03424579	2.345
CPRP	45	5	1.07	0.02465579	0.02458083	3.040	0.02129696	0.02142663	6.089
	120	10	3.50	0.01165195	0.01166741	1.327	0.01055419	0.01057317	1.798
	500	6	4.28	0.00166994	0.00167389	2.365	0.00153944	0.00154153	1.358
	12	8	0.61	0.14334110	0.14334916	0.056	0.12171494	0.12156599	1.224
	18	15	1.41	0.12726978	0.12728937	0.154	0.11291462	0.11288638	0.250
PENNZ	40	12	1.68	0.04516983	0.04519063	0.460	0.04031014	0.04036518	1.365
	200	12	3.75	0.00719969	0.00720202	0.324	0.00658494	0.00658984	0.744
	600	6	3.25	0.00133440	0.00133627	1.401	0.00122894	0.00123036	1.155

Table 4: Error analysis: comparison between the full and reduced models

	M	L	p_h	N° of Iterations		cpu time (s)	
			(GPA)	Full	Red.	Full	Red.
	12	12	0.70	13	16	4.20	0.45
	17	15	1.04	23	38	7.60	1.10
CPRI	45	5	0.57	11	11	3.80	0.30
	100	10	1.69	17	17	5.40	0.68
	600	8	3.31	24	16	8.20	0.51
	13	8	0.92	14	14	4.70	0.38
	40	9	1.82	13	20	7.10	0.59
CPRP	45	5	1.07	8	10	2.90	0.28
	120	10	3.50	16	17	5.20	0.71
	500	6	4.28	27	25	10.0	0.99
	12	8	0.61	14	16	4.60	0.44
	18	15	1.41	49	50	15.0	1.50
PENNZ	40	12	1.68	27	29	8.40	0.86
	200	12	3.75	25	27	8.30	0.81
	600	6	3.25	30	24	11.0	1.00

Table 5: Performance analysis: comparison between the full and reduced models

Finally, note the relatively small number of iterations required for a converged solution using this full-system damped-Newton approach. This clearly highlights the attractive feature of this type of approach as indicated previously.

5 Conclusion

This paper presents a novel reduced model for a fast and robust solution of EHL problems. The developed approach is applied to the isothermal Newtonian line contact case, operating under steady-state regime. The model is based on a Full-System finite element resolution of the EHL equations: Reynolds, linear elasticity and load balance. A model reduction technique is derived to reduce the size of the

linear elasticity problem. This leads to a significant reduction in the size of the global discrete system of equations, leading to a considerable reduction in cpu time. The model is shown to be robust, allowing the solution of the EHL problem over a wide range of operating conditions. Its complexity is shown to be approximately *O(n)*. The relative error in the film thickness results for the reduced model compared to the full one is shown to be of the order of only 1‰ under a wide range of operating conditions.

Although only isothermal Newtonian line contacts are considered in this work, the developed approach can be extended to more general cases. In fact, this work aimed to prove the feasibility of this approach and demonstrate its attractive cpu time reduction feature. The latter is of minor importance in the line contact case, since the corresponding solution can be obtained relatively fast even in the full model case. This feature would be of much greater importance for more computationally demanding applications e.g. transient regime, point contacts… The extension of the reduced model to these cases is planned for future work.

Nomenclature

A_1, A_2 : Modified WLF model constant parameters
B_1, B_2 : Modified WLF model constant parameters
C_1, C_2 : Modified WLF model constant parameters
E_i : Young's modulus of solid body *i*
E_{eq} : Equivalent Young's modulus
F : External load
H : Dimensionless film thickness
H_0 : Dimensionless film thickness constant parameter
L : Dimensionless Moes material properties parameter
M : Dimensionless Moes load parameter
N_{1D} : Number of dof in the *1D* hydrodynamic problem
N_{2D} : Number of dof in the *2D* linear elasticity problem
N_{dof} : Total number of dof of the full model
$\tilde{N}_{dof}$: Total number of dof of the reduced model
N_m : Number of basis functions employed in the reduced model
P : Dimensionless pressure
Pe : Peclet number
R : Cylindrical roller radius
S_P : Pressure solution space
S_U : Elastic deflection solution space
$\tilde{S}_U$: Elastic deflection reduced solution space
T_0 : Ambient temperature
$T_g(0)$: Lubricant's ambient pressure glass transition temperature
X : Dimensionless space coordinate
a : Hertzian contact half-width
p : Pressure
p_h : Hertzian pressure

u_i : Surface velocity of solid body *i*
u_m : Mean entrainment speed
α^* : Equivalent pressure-viscosity coefficient
μ_g : Lubricant's viscosity at glass transition temperature
μ_R : Lubricant's reference viscosity
$\bar{\mu}$: Lubricant's dimensionless viscosity
v_i : Poisson's coefficient of solid body *i*
v_{eq} : Equivalent Poisson's coefficient
φ^i : Basis function *i*
$\bar{\rho}$: Lubricant's dimensionless density
ρ_R : Lubricant's reference density

Subscripts

e : Elastic
h : Hydrodynamic
l : Load balance

Dimensionless parameters

$$X = \frac{x}{a} \qquad P = \frac{p}{p_h} \qquad \bar{\rho} = \frac{\rho}{\rho_R} \qquad \bar{\mu} = \frac{\mu}{\mu_R} \qquad H = \frac{hR}{a^2}$$

References

[1] Dowson D. and Higginson G. R. – A Numerical Solution of the Elastohydrodynamic Problem. *J. Mech. Eng. Sci.*, 1959, vol. 1, n° 1, pp. 6-15.

[2] Hamrock B. J. and Dowson D. – Isothermal Elastohydrodynamic Lubrication of Contacts, Part I – Theoretical Formulation. *ASME J. of Lubr. Techn.*, 1976, vol. 98, n° 2, pp. 223-229

[3] Rohde S. M. and Oh K. P. – A Unified Treatment of Thick and Thin Film Elastohydrodynamic Problems by Using Higher Order Element Methods. *Proc. Roy. Soc. London*, 1975, Part A, vol. 343, pp. 315-331.

[4] Houpert L. G. and Hamrock B. J. – Fast Approach for Calculating Film Thicknesses and Pressures in Elastohydrodynamically Lubricated Contacts at High Loads. *ASME J. of Tribol.*, 1986, vol. 108, pp. 411-420.

[5] Hughes T. G., Elcoate C. D. and Evans H. P. – Coupled Solution of the Elastohydrodynamic Line Contact Problem Using a Differential Deflection Method. *Proc. IMechE J. Mech. Engnrng. Sc.*, 2000, Part C, vol. 214, pp. 585-598.

[6] Evans H. P. and Hughes T. G. – Evaluation of Deflection in Semi-Infinite Bodies by a Differential Method. *Proc. IMechE J. Mech. Engnrng. Sc.*, 2000, Part C, vol. 214, pp. 563-584.

[7] W. Habchi, D. Eyheramendy, P. Vergne, G. Morales-Espejel, "Stabilized Finite Elements for Elastohydrodynamic Lubrication Problems", in M. Papadrakakis, B.H.V. Topping, (Editors), "Proceedings of the Sixth International Conference on Engineering Computational Technology", Civil-Comp Press, Stirlingshire, UK, Paper 19, 2008. doi:10.4203/ccp.89.19.

[8] Habchi W. – A Full-System Finite Element Approach to Elastohydrodynamic Lubrication Problems: Application to Ultra-Low-Viscosity Fluids, *PhD Thesis,* 2008, INSA de Lyon, France.

[9] Habchi W., Eyheramendy D., Vergne P. and Morales-Espejel G., "Stabilized Fully-Coupled Finite Elements for Elastohydrodynamic Lubrication Problems", *Int. J. of Adv. in Eng. Software*, (Article in Press), doi:10.1016 /j.advengsoft.2010.09.010.

[10] Wu S. R. – A Penalty Formulation and Numerical Approximation of the Reynolds-Hertz Problem of Elastohydrodynamic Lubrication. *Int. J. Engnrng. Sci.*, 1986, vol. 24 (6), pp. 1001-1013.

[11] Reynolds O. – On The Theory of the Lubrication and its Application to Mr Beauchamp Tower's Experiments, Including an Experimental Determination of the Viscosity of Olive Oil. *Phil. Trans. R. Soc.*, 1886, vol. 177, pp.157-234.

[12] Hertz H. – Uber die Berührung fester Elastischer Körper. *J. reine und angew. Math.*, 1881, vol. 92, pp. 156-171.

[13] Yasutomi S., Bair S. and Winer W. O. - An Application of a Free-Volume Model to Lubricant Rheology, (1) Dependence of Viscosity on Temperature and Pressure. *ASME J. of Tribol.*, 1984, vol. 106, pp. 291-312.

[14] Dowson D. and Higginson G. R. – Elastohydrodynamic Lubrication. The Fundamental of Roller and Gear Lubrication. *Oxford, Pergamon* (1966).

[15] Deuflhard P. – Newton Methods for Nonlinear Problems, Affine Invariance and Adaptive Algorithms. *Springer*, Germany, 2004.

[16] Davis T. A. and Duff I. S. - An Unsymmetric-Pattern Multifrontal Method for Sparse LU Factorization, *SIAM Journal on Matrix Analysis and Applications*, vol. 18, no. 1, pp. 140-158, 1997.

[17] Noor A. K. – Recent Advances and Applications of Reduction Methods. *Appl. Mech. Rev.,* vol. 47 (5), pp. 125-145, 1994.

[18] Qu Z.Q. – Model Order Reduction Techniques with Applications in Finite Element Analysis. *Springer*, UK, 2004.

[19] Wilson E. L., Yuan M. W. and Dickens J. M. – Dynamic Analysis by Direct Superposition of Ritz Vectors. *Earthquake Engineering and Structural Dynamics,* vol. 10, pp. 813-821, 1982.

[20] Habchi. W. and Issa J. - Fast and Reduced Full-System Finite Element Solution of Elastohydrodynamic Lubrication Problems: Line Contacts (Submitted to *Int. J. of Adv. in Eng. Software*)

[21] Moes H. – Optimum Similarity Analysis with Applications to Elastohydrodynamic Lubrication. *Wear*, vol. 159, pp. 57-66, 1992.